Signal transduction pathways activated by insulin-like peptide 5 (INSL5) at the relaxin family peptide receptor 4 (RXFP4).

Sheng Y. Ang[1]
Dana S. Hutchinson[1,2]
Nitin Patil[3]
Bronwyn A. Evans[1]
Ross A.D. Bathgate[3]
Michelle L. Halls [1]
Mohammed A. Hossain[3]
Roger J. Summers[1]
Martina Kocan [1]

[1]Drug Discovery Biology, Monash Institute of Pharmaceutical Sciences, Monash University, Parkville, Victoria, Australia (S.Y.A., D.S.H., B.A.E., M.K., R.J.S.); [2]Department of Pharmacology, Monash University, Clayton, Victoria, Australia (D.S.H.); [3]The Florey Institute of Neuroscience and Mental Health, University of Melbourne, Parkville, Victoria, Australia (N.P., R.A.D.B., A.M.H.) and Department of Biochemistry and Molecular Biology, University of Melbourne (R.A.D.B.)

This is the author manuscript accepted for publication and has undergone full peer review but has not been through the copyediting, typesetting, pagination and proofreading process, which may lead to differences between this version and the Version of Record. Please cite this article as doi: 10.1111/bph.13522

Corresponding authors: Prof Roger Summers & Dr Martina Kocan

Drug Discovery Biology

Monash Institute of Pharmaceutical Sciences

Monash University

381 Royal Parade

Parkville VIC 3052 Australia

Email: roger.summers@monash.edu; martina.kocan@monash.edu

Phone: +61 (0)3 9905 9066/9056

Running title: RXFP4 signal transduction pathways

Number of text pages: 27

Number of tables: 1

Number of Figures: 7

Number of references: 47

Number of words in Abstract: 250

Number of words in Introduction: 571

Number of words in Discussion: 1614

Abbreviations

BrdU, 5-bromo-2'-deoxyuridine

CRE, cAMP response element

GLP-1, glucagon-like peptide 1

GRK2, G protein receptor kinase 2

INSL5, Insulin-like peptide 5

mTORC, mammalian target of rapamycin complex

PTX, pertussis toxin

RXFP4, relaxin family peptide receptor 4

S6RP, S6 ribosomal protein

Keywords

Insulin-like peptide 5, relaxin family peptide receptor 4, intracellular signalling

BACKGROUND AND PURPOSE

Insulin-like peptide 5 (INSL5) is a two-chain, three-disulphide bonded peptide of the insulin/relaxin superfamily, uniquely expressed in enteroendocrine L-cells of the colon. It is the cognate ligand of relaxin family peptide receptor 4 (RXFP4) that is mainly expressed in the colorectum and enteric nervous system. This study identifies new signalling pathways activated by INSL5 acting on RXFP4.

EXPERIMENTAL APPROACH

INSL5/RXFP4 signalling was investigated using AlphaScreen® proximity assays. RXFP4 recruitment of $G\alpha_{i/o}$ proteins was determined by rescue of pertussis toxin (PTX)-inhibited cAMP and ERK1/2 responses following transient transfection of PTX-insensitive $G\alpha_{i/o}$ C351I mutants. Cell proliferation was studied using bromodeoxyuridine cell proliferation ELISA. Real-time BRET was used to examine RXFP4 interactions with β-arrestins, G protein-coupled receptor kinase 2 (GRK2), KRas and Rab5a. Gene expression was investigated using real-time quantitative PCR. Insulin release was measured using HTRF and intracellular Ca^{2+} flux monitored in a Flexstation® using Fluo-4-AM.

KEY RESULTS

INSL5 inhibited forskolin-stimulated cAMP accumulation and increased phosphorylation of ERK1/2, p38MAPK, Akt-Ser473, Akt-Thr308 and S6 ribosomal protein (S6RP). cAMP and ERK1/2 responses were abolished by PTX and rescued by $mG\alpha_{oA}$, $mG\alpha_{oB}$ and $mG\alpha_{i2}$ and to a lesser extent $mG\alpha_{i1}$ and $mG\alpha_{i3}$. RXFP4 interacted with GRK2 and β-arrestins, moved towards Rab5a and away from KRas, indicating internalisation following receptor activation. INSL5 treatment inhibited glucose-stimulated insulin secretion and Ca^{2+} mobilisation in MIN6 insulinoma cells, and forskolin-stimulated cAMP accumulation in NCI-H716 enteroendocrine cells.

Knowledge of signalling pathways activated by INSL5 at RXFP4 is essential for understanding the biological roles of this novel gut hormone.

Introduction

Insulin-like peptide 5 (INSL5) is a two-chain, three disulfide-bond peptide with a striking structural similarity to insulin. It was identified in 1999 as a member of the insulin/relaxin superfamily by searching the expressed sequence tags (EST) database (Conklin et al., 1999; Hsu, 1999). Subsequently, INSL5 was identified as the cognate ligand for relaxin family peptide receptor 4 (RXFP4; formerly GPR100/GPCR142, Liu et al., 2005; Alexander et al., 2015) based on matching pharmacology and ligand-receptor distribution in peripheral tissues. Although relaxin-3, a neuropeptide that is highly expressed in the nucleus incertus, is also a full agonist at RXFP4 (Liu et al., 2005; Smith et al., 2010), it is not regarded as the physiological ligand due to disparate anatomical expression of the peptide and receptor (Boels and Schaller, 2003; Liu et al., 2005; Sutton et al., 2006).

More recently, INSL5 was identified as a novel gut hormone that is expressed in enteroendocrine L-cells together with glucagon-like peptide 1 (GLP-1) and peptide YY, with high levels of expression in the colon and proximal rectum (Mashima et al., 2013; Thanasupawat et al., 2013; Grosse et al., 2014). Mice that were administered INSL5 i.p. displayed a dose-dependent increase in food intake that was absent in RXFP4$^{-/-}$ mice, suggesting that INSL5 is an orexigenic gut hormone acting via RXFP4 (Grosse et al., 2014). In addition, a recent study has suggested that INSL5 augments glucose-simulated insulin secretion from MIN6 pancreatic β-cells and GLP-1 release from murine enteroendocrine GLUTag cells (Luo et al., 2015), indicating that INSL5-RXFP4 may constitute a novel incretin axis involved in the regulation of metabolism and energy balance.

Relatively little is known of the signal transduction pathways activated by RXFP4, but the receptor is known to couple to pertussis toxin (PTX)-sensitive $G\alpha_{i/o}$ proteins to inhibit forskolin-stimulated cAMP accumulation (Liu et al., 2003; 2005; Belgi et al., 2011). RXFP4 also activates extracellular signal-regulated kinases 1 and 2 (ERK1/2) in a heterologous system overexpressing the receptor (Belgi et al., 2013) and in MIN6 and GLUTag cells endogenously expressing RXFP4 (Luo et al., 2015). RXFP4 does not appear to couple to $G\alpha_q$ proteins since INSL5 evokes an intracellular Ca^{2+} response only in systems co-transfected with the promiscuous $G\alpha_{16}$ (Liu et al., 2003; 2005).

In this study, we present evidence that RXFP4 stimulation by INSL5 activates intracellular signalling pathways in addition to ERK1/2 and inhibition of cAMP, in particular p38MAPK, Akt and S6 ribosomal protein (S6RP), in Chinese hamster ovary (CHO) cells stably expressing RXFP4. The pattern of signalling activation suggests that RXFP4 is involved in the control of cellular growth and proliferation, and this was supported by increased 5-bromo-2'-deoxyuridine (BrdU) incorporation following stimulation with INSL5. We were also able to show that INSL5 inhibits glucose-stimulated insulin secretion and Ca^{2+} mobilisation in MIN6 insulinoma cells and cAMP accumulation in NCI-H716 enteroendocrine cells. In CHO-RXFP4 cells, pertussis toxin-insensitive G protein mutants were used to identify the $G\alpha_{i/o}$ subunits involved in activation of RXFP4-mediated ERK1/2 and inhibition of cAMP signalling. Bioluminescence Resonance Energy Transfer (BRET) was used to show that agonist-activated RXFP4 interacts with GRK2, β-arrestin-1 and -2 and moves towards the early endosome marker Rab5a. Over the same time period RXFP4 moves away from the plasma membrane marker KRas, suggesting that following ligand stimulation, RXFP4 undergoes classical GRK and β-arrestin mediated receptor internalisation, followed by sequestration to an early endosomal compartment. Unravelling the signalling profile of drugs acting at RXFP4 is essential for development of therapies targeting this receptor.

Materials and Methods

Cell culture and transient transfection

CHO-K1 cells stably expressing human RXFP4 (CHO-RXFP4) were grown and maintained in 175-cm^2 flasks in DMEM/F-12 medium supplemented with 5% (v/v) foetal bovine serum (FBS) at 37°C in humidified air containing 5% CO_2. MIN6 murine insulinoma cells (a gift from A/Prof Helen Thomas, St Vincent's Institute of Medical Research, Melbourne, Australia) were grown and maintained in 175-cm^2 flasks in high glucose DMEM supplemented with 15% FBS, 55 μM β-mercaptoethanol, 25 mM HEPES, 100 IU/ml penicillin and 100 μg/ml streptomycin. NCI-H716 human adenocarcinoma cells, an established model of L-type enteroendocrine cells, were grown in high glucose RPMI supplemented with 10% FBS, 100 IU/ml penicillin and 100 μg/ml streptomycin. For the constructs outlined below, transient transfections were carried out using Lipofectamine 2000 (Thermo Fisher Scientific, Scoresby, VIC Australia) as per the manufacturer's protocol. After 24 hours, transfected cells were trypsinised, seeded onto 96-well plates and used within 24 hours.

Constructs

cDNA constructs for human RXFP4 and PTX-insensitive $G\alpha_{i/o}$ subunit mutants were from the cDNA Resource Center (Bloomsberg, PA, USA; http://www.cdna.org). These G protein α-subunits contain a Cys^{351} to Ile^{351} mutation (C351I) that renders them insensitive to ADP-ribosylation by PTX (Bahia et al., 1998). Human RXFP4 sequence was amplified from RXFP4-pcDNA3.1+ using the forward primer 5'-GGGGACAAGTTTGTACAAAAAAGCAGGCTTCCACCATGCCCACACTCAATACTTCT-3' (start codon underlined) and reverse primer 5'-GGGGACCACTTTGTACAAGAAAGCTGGGTCCCCGGGTGTCCCTCTGTC-3', containing attB1 and attB2 sites respectively. The PCR product was gel purified and cloned into pDONR201 vector (Thermo Fisher) using BP clonase II to create an entry clone containing attL1- and attL2-flanked RXFP4 sequence. An LR recombination reaction was performed between the entry clone and a destination vector containing attR1-, attR2- and Rluc8 sequence to create the RXFP4-Rluc8 tagged construct. The RXFP4-Rluc8 insert was sequenced on both strands (Australian Genome Research Facility, Parkville, VIC Australia). Human β-arrestin 1-Venus, β-arrestin 2-Venus and GRK2-Venus constructs have been described previously (Kocan et al., 2008; Jensen et al., 2013; Kocan et al., 2014). KRas-Venus and Rab5a-Venus constructs were kindly provided by Prof. Nevin Lambert (Georgia Regents University, USA).

Protein phosphorylation

Phosphorylation of ERK1/2 (Thr202/Tyr204), p38MAPK (Thr180/Tyr182), Akt (Thr308 and Ser473) and S6RP (Ser235/236) were determined using AlphaScreen SureFire® kits (PerkinElmer, Glen Waverley VIC, Australia). Cells were seeded onto 96-well plates at a density of 50,000 – 60,000 cells per well and incubated overnight in complete media to allow cell adhesion. The following day, cells were serum-starved for 4-6 hours to reduce basal phosphorylation levels and then stimulated with human or mouse INSL5 (hINSL5 or mINSL5, 200 nM each) for up to 45 min for time-course studies, or with increasing concentrations of the peptides (10^{-11} to $10^{-6.5}$ M) for concentration-response studies for the indicated time periods. For inhibitor studies, cells were pre-incubated with inhibitors for 30 min except PTX where cells were exposed for 18 h. After stimulation, cells were lysed and frozen at -80°C. For assay, 4 µl of thawed cell lysate was added to a white 384-well microplate (ProxiPlate; PerkinElmer) containing 5 µl acceptor beads mix (40 parts reaction buffer/10 parts activation buffer/1 part protein A acceptor beads) and incubated for 2 hours at room temperature. Then, 2 µl donor bead mix (20 parts dilution buffer/1 part streptavidin-coated donor beads) was added and incubated for 2 hours at room temperature. All additions and incubations were carried out under low light conditions to avoid photobleaching. Plates were read using an Envision multilabel plate reader (PerkinElmer; excitation wavelength = 680 nm; emission wavelength = 520 - 620 nm).

Inhibition of cAMP accumulation

The amount of cAMP generated by forskolin and its inhibition by INSL5 peptides was measured using an AlphaScreen cAMP kit (PerkinElmer). Cells were seeded and serum starved as described above for protein phosphorylation assays. Following serum starvation, medium was changed to HBSS supplemented with 500 mM IBMX, 5 mM HEPES and 0.1% (w/v) BSA and equilibrated for 1 hour at 37°C. Cells were stimulated with hINSL5 or mINSL5 (10^{-11} to $10^{-6.5}$ M) for 15 min and then with forskolin (3 µM) for 30 min. Cells were lysed in buffer containing 0.3% Tween-20, 5 mM HEPES and 0.1% (w/v) BSA and frozen at -80^{O}C, followed by fluorescence detection according to the protocol provided by the manufacturer. In brief, 5 µl of cell lysate was added to a white 384-well microplate (OptiPlate; PerkinElmer) containing 5 µl acceptor beads mix (1U acceptor beads in 5 µl lysis buffer) and incubated for 30 min at room temperature. Then, 15 µl of donor beads mix (1U

biotinylated cAMP/1U donor beads in 15 µl lysis buffer) was added and incubated for 1 hour at room temperature. Fluorescence was measured using an Envision plate multilabel plate reader (PerkinElmer; excitation wavelength = 680 nm; emission wavelength = 520 - 620 nm).

Cell proliferation

Cells were seeded onto 96-well clear-bottom black plates at a density of 5,000 cells per well in serum-free DMEM/F-12 medium. The following day cells were treated with hINSL5 or mINSL5 (10^{-12} to 10^{-8} M) for 24 h, before labeling with BrdU overnight. The amount of BrdU incorporated into cellular DNA, a marker of cell proliferation, was measured using a BrdU cell proliferation (chemiluminescent) ELISA kit (Roche Diagnostics, Mannheim, Germany) according to the manufacturer's instructions.

Real-time kinetic BRET studies

CHO-K1 cells grown on 6-well plates were transiently co-transfected with cDNAs encoding RXFP4-Rluc8 and β-arrestin 1-Venus, β-arrestin 2-Venus, GRK2-Venus or KRAS-Venus. 24 hours after transfection, cells were harvested and seeded onto 96-well opaque white plates in phenol-red free DMEM with 5% FBS and grown overnight. The next day, coelenterazine *h* (5 µM) was added to cells, followed by stimulation with hINSL5 or mINSL5 (200 nM each). Dual light emission [480 nm (donor wavelength window); 530 nm (acceptor wavelength window)] was simultaneously recorded in real-time using a LUMIstar Omega microplate reader (BMG Labtech, Ortenberg, Germany) before and after addition of ligands.

RNA purification and real-time quantitative PCR

Total RNA was isolated from MIN6 cells using RNeasy mini RNA purification kit and treated with RNase-free DNase (Qiagen, Hilden, Germany) as per manufacturer's instruction. Purified RNA (500 ng) was reverse transcribed (iScript Reverse Transcription Supermix Bio-Rad, CA, USA), the cDNA diluted 1:40, and 4 µl of the diluate used for PCR 10 µl reactions containing 0.5 µl Taqman primers and probes (*Rxfp4*: Mm00731536_s1, *Glp1r*: Mm00445292; reference gene *Actb*: Mm00607939; Thermo Fisher Scientific), 5 µl of Taqman Fast Advanced Master Mix (Thermo Fisher Scientific) and 0.5 µl Ultrapure DNase/RNase-free H_2O (Thermo Fisher Scientific). Real-time quantitative PCR (40 cycles) was performed with a Mastercycler ep Realplex (Eppendorf, Hamburg, Germany). After

initial denaturation at 95°C for 30 sec, fluorescence was detected over 40 cycles (95°C for 5 sec, 60°C for 30 sec).

Insulin secretion assay

MIN6 cells were seeded onto 96-well plates at 50,000 – 60,000 cells per well and allowed to grow overnight. The next day, the cells were equilibrated for 2 hours in KRB buffer, followed by stimulation in either 0 mM or 10 mM glucose in the absence and presence of increasing concentrations of mINSL5 (0.1 – 200 nM) for 2 hours. Supernatants were collected and the insulin secreted measured using a HTRF insulin kit (Cisbio, Codolet, France).

Intracellular Ca^{2+} mobilisation

MIN6 cells were seeded onto 96-well plates as above. Following serum starvation, cells were incubated in HBSS supplemented with 2 mM probenecid, 0.5% (w/v) BSA and 1 μM Fluo 4-AM (Thermo Fisher Scientific) for 30 min, washed and equilibrated for a further 30 min in buffer without Fluo 4-AM. mINSL5 was added in the Flexstation (Molecular Devices, Sunnyvale CA) and real-time fluorescence measured every 3 s for 10 min (excitation = 485 nm; emission = 520 nm).

Data and statistical analysis

Time-course and concentration-response studies for protein phosphorylation were expressed as fold change of fluorescence over that of vehicle control, for inhibition of cAMP accumulation as % of the forskolin response, or for cell proliferation as % of the response to 10% FBS and plotted using Prism (v6.0; GraphPad software, San Diego, CA, USA). All concentration-response curves were fitted using a three parameter Hill equation within Prism. pEC_{50} values of mouse and human INSL5 were compared using two-way ANOVA with post-hoc Tukey's multiple comparisons test. For inhibitor studies, data were expressed as fold change of fluorescence over that of vehicle control and statistical analysis performed using repeated-measures two-way ANOVA followed by Dunnett's multiple comparisons test. Ligand-induced BRET ratio was calculated by subtracting the acceptor/donor wavelength ratio (530 nm/480 nm) of vehicle-treated cells from the corresponding wavelength ratio of ligand-treated cells, and normalised to the value at t=0 min (prior to addition of vehicle or ligand) (Kocan and Pfleger, 2011; Kocan et al., 2014). For real-time quantitative PCR, data were expressed

as the relative abundance of the gene of interest relative to the reference gene, *Actb* using the following equation:

$$2^{-\Delta Ct} * 1000$$

$$\text{where } \Delta Ct = Ct_{gene\text{-}of\text{-}interest} - Ct_{ACTB}$$

For the Ca^{2+} mobilisation study, data were expressed as baseline-subtracted raw fluorescence units, and areas under the Ca^{2+} curves were calculated using the built-in function in Prism.

Materials

Human and mouse INSL5 were synthesised and purified at The Florey Institute of Neuroscience and Mental Health (Melbourne, Australia) as described previously (Hossain et al., 2008; Belgi et al., 2013). For some experiments, mouse INSL5 purchased from Phoenix Pharmaceuticals (Burlingame, CA, USA) was used, following verification that it had the same potency as INSL5 prepared in-house (data not shown). FBS, HEPES, DMEM Ham's/F-12, HBSS and PTX were all from Life Technologies (Carlsbad, CA, USA). IBMX was from Sigma-Aldrich (Castle Hill, NSW, Australia). Coelenterazine *h* was purchased from Nanolight (Pinetop, AZ, USA).

Results

INSL5 activated ERK1/2 phosphorylation in a heterologous system expressing RXFP4 (Belgi et al., 2013), and in pancreatic MIN6 and enteroendocrine GLUTag cells that endogenously express the receptor (Luo et al., 2014). Here, we confirm activation of ERK1/2 but in addition demonstrate that RXFP4 activates Akt, p38MAPK and S6RP, that are signalling proteins implicated in a wide variety of cellular functions including growth, survival, proliferation and/or metabolism.

INSL5 promotes ERK1/2, Akt, p38MAPK and S6RP phosphorylation, and inhibits forskolin-stimulated cAMP accumulation

Treatment times were optimised for each assay (Fig S1) and neither mINSL5 nor hINSL5 had any effect in any assay carried out with untransfected CHO-K1 cells (Fig S2). Previously it has been shown that mINSL5 has a higher potency than hINSL5 in CHO-RXFP4 cells in assays measuring activation of ERK1/2 and inhibition of cAMP production (Belgi et al., 2013). We confirmed these findings and also showed for phosphorylation of Akt, p38MAPK and S6RP, that mINSL5 consistently had greater potency than hINSL5 (Fig. 1, A-F; Table 1). mINSL5 potencies ranged from 8.86 for inhibition of forskolin-stimulated cAMP accumulation down to 7.80 and 7.86 for phosphorylation of Akt at Thr308 and Ser473 respectively, reflecting differences in coupling efficiency between the activated receptor and each signalling pathway. The rank order of potency was cAMP inhibition > S6RP = ERK1/2 > p38MAPK > Akt Ser473 = Akt Thr308. No accurate pEC_{50} values could be determined for hINSL5-stimulated Akt phosphorylation. The pEC_{50} values of hINSL5 for cAMP, ERK1/2, p38 MAPK and S6RP were not significantly different, clustering between 7.46 and 7.62 ($p > 0.05$). On the other hand, pEC_{50} values for mINSL5 were significantly different between Akt Thr308 and cAMP ($p < 0.0001$), S6RP ($p < 0.01$) and ERK1/2 ($p < 0.05$), and Akt Ser473 with cAMP ($p < 0.01$).

RXFP4 activation of ERK1/2 requires G $\alpha_{i/o}$, MEK and Src and is partially regulated by PI3K but does not depend on activation of mTOR

$G\alpha_{i/o}$ proteins and MEK1/2 (a kinase immediately upstream of ERK1/2) have obligatory roles for RXFP4 activation of p-ERK1/2, since PTX ($G\alpha_{i/o}$ inhibitor; 100 ng/ml; 18 h) or U0126 (MEK inhibitor; 10 μM; 30 min) both completely abrogated the INSL5-induced p-ERK1/2 response in CHO-RXFP4 cells ($p < 0.0001$, n = 5, Fig 2A). Src is often involved in GPCR-mediated ERK1/2 signalling (Luttrell et al., 1996; Cao, 2000) and PP2 (selective Src family kinase inhibitor; 10 μM; 30 min) completely inhibited the INSL5-stimulated ERK1/2 response ($p < 0.0001$; n = 5; Fig 2A), suggesting that Src family kinases have a critical role in activation of ERK1/2 by RXFP4. The PI3K inhibitor LY294002 (10 μM; 30 min) partially inhibited the ERK1/2 response to INSL5 by ($p < 0.01$; n = 5; Fig 2A) suggesting that PI3K may contribute to the ERK1/2 response. mTORC1 was examined using the mTOR inhibitors KU0063794 (1 μM; 30 min) or rapamycin (100 nM; 30 min), since cross-regulation can occur between the Ras-ERK and PI3K-Akt pathways (Mendoza et al., 2011). Neither KU0063794 nor rapamycin ($p > 0.05$; n =5; Fig 2A) inhibited the INSL5-mediated

ERK1/2 response, with KU0063794 in fact causing a slightly elevated response ($p < 0.05$; n = 5; Fig 2A), implying that RXFP4 activation of ERK1/2 does not involve mTORC1.

RXFP4 activation of Akt Thr308 and Akt Ser473 requires $G\alpha_{i/o}$, Src, PI3K and mTORC2 but does not involve MEK1/2 or mTORC1

Activation of Akt by INSL5 in CHO-RXFP4 requires $G\alpha_{i/o}$ proteins and Src, since PTX (100 ng/ml; 18 h; n = 5) and PP2 (10 μM; 30 min; n = 6) completely inhibited Akt phosphorylation at Thr308 ($p < 0.001$ and $p<0.0001$, respectively; Fig 2B) and Ser473 ($p < 0.0001$ each; Fig 2C). PI3K has an obligatory role in activation of Akt by INSL5 as LY294002 (10 μM; 30 min) completely blocked responses at Thr308 ($p < 0.0001$; n = 7; Fig 2B) and Ser473 ($p < 0.0001$; n = 7; Fig 2C). Conversely, MAPK signalling does not play a part in the INSL5-mediated Akt response because inhibition of MEK1/2 with U0126 (10 μM; 30 min) did not alter the response at either phosphorylation site ($p > 0.05$; n = 6; Fig 2B, C). Interestingly, activation of Akt by INSL5 at Thr308 and Ser473 was sensitive to inhibition by KU0063794 (1 μM; 30 min; $p < 0.0001$; n = 5) but completely resistant to rapamycin (100 nM; 30 min; $p > 0.05$; n=5; Fig 2B, C). This implies that mTORC2, but not mTORC1, is required for the INSL5-mediated Akt response, as KU0063794 inhibits both mTORC1 and mTORC2 (García-Martínez et al., 2009) while rapamycin selectively inhibits only mTORC1 (Loewith et al., 2002).

RXFP4 activates S6RP via pathways involving $G\alpha_{i/o}$, Src, MEK1/2, PI3K and mTORC1

S6RP, a protein component of the 40S ribosomal subunit, is a downstream effector of the ribosomal S6 kinase S6K, which is activated by the Akt-mTOR pathway (Ruvinsky and Meyuhas, 2006). Activation of S6RP by INSL5 in CHO-RXFP4 absolutely requires $G\alpha_{i/o}$ proteins and Src family kinases since there was complete inhibition of the S6RP response by PTX (100 ng/ml; 18 h; n = 5) and PP2 (10 μM; 30 min; n = 5), respectively ($p < 0.0001$; Fig 2D). In addition, MAPK signalling can also influence S6RP activation (Roux et al., 2007). Inhibition of MEK1/2 with U0126 (10 μM; 30 min; n = 6) inhibited INSL5-stimulated S6RP activation by ~50% in CHO-RXFP4 cells ($p < 0.001$; Fig 2D). Inhibition of PI3K by LY294002 (10 μM; 30 min; n = 6) and mTOR by KU0063794 (1 μM; 30 min; n = 5) or rapamycin (100 nM; 30 min; n = 5) also completely abolished INSL5-stimulated S6RP activation ($p < 0.0001$ each; Fig 2D), suggesting that the PI3K-mTORC1 pathway is pivotal in mediating this response in CHO-RXFP4.

RXFP4 utilises multiple $G\alpha_{i/o}$ subunits to inhibit forskolin-stimulated cAMP accumulation and activate ERK1/2 in CHO-RXFP4 cells

RXFP4 inhibits forskolin-stimulated cAMP production (Liu et al., 2005; Belgi et al., 2013; Shabanpoor et al., 2013), suggesting that the receptor couples to $G\alpha_{i/o}$. However, whether RXFP4 utilises a selective subset or all of the $G\alpha_{i/o}$ subunits remains unknown. This was determined for INSL5-mediated ERK1/2 activation and inhibition of cAMP in CHO-RXFP4 cells by transiently transfecting cells with PTX-insensitive $G\alpha_{i/o}$ mutants ($mG\alpha_{oA}$, $mG\alpha_{oB}$, $mG\alpha_{i1}$, $mG\alpha_{i2}$ or $mG\alpha_{i3}$) followed by treatment with PTX. In essence, a rescue of cAMP or ERK1/2 responses normally suppressed by PTX in the presence of exogenous $G\alpha_{i/o}$ mutants reveals the pattern of $G\alpha_{i/o}$ activation by RXFP4.

We first showed that INSL5-mediated inhibition of forskolin-stimulated cAMP accumulation was abolished by PTX in mock-transfected CHO-RXFP4 cells ($p > 0.05$; $n = 7$; Fig. 3A), confirming the involvement of $G\alpha_{i/o}$ in RXFP4 signal transduction. We then demonstrated that cAMP responses could be rescued in PTX-treated cells singly transfected with each $G\alpha_{i/o}$ mutant. The degree of cAMP rescue ranged from 83 ± 16% for $mG\alpha_{oB}$ ($p < 0.001$; $n = 6$; Fig 3C), 58.7 ± 3.6% for $mG\alpha_{oA}$ ($p < 0.01$; $n = 7$; Fig 3B), 51.6 ± 6.2% for $mG\alpha_{i2}$ ($p < 0.01$; $n = 7$; Fig 3E), 49.2 ± 14% for $mG\alpha_{i1}$ ($p < 0.01$; $n = 7$; Fig 3D) and 40.3 ± 4.7% for $mG\alpha_{i3}$ ($p < 0.01$; $n = 6$; Fig 3F). When similar studies were performed for INSL5-medicated ERK1/2 activation, the degree of rescue was less pronounced across all the $G\alpha_{i/o}$ mutants tested. ERK1/2 response rescue varied from 24.8 ± 6.2% for $mG\alpha_{oB}$ ($p < 0.05$; $n = 5$; Fig 3I), 23.9 ± 5.6% for $mG\alpha_{oA}$ ($p < 0.01$; $n = 5$; Fig 3H), 19.8 ± 4.8% for $mG\alpha_{i2}$ ($p < 0.01$; $n = 5$; Fig 3K), 10.14 ± 2.8% for $mG\alpha_{i3}$ ($p < 0.05$; $n = 5$; Fig 3L) to 5.25 ± 2.4% for $mG\alpha_{i1}$ (non-significant, $p > 0.05$; $n = 5$; Fig 3J). RXFP4 was therefore able to engage multiple $G\alpha_{i/o}$ isoforms to promote cAMP inhibition and ERK1/2 activation, but did indicate a preference for $G\alpha_{oA,}$ $G\alpha_{oB}$ and $G\alpha_{i2}$.

INSL5 promotes cell proliferation in vitro

Since INSL5 activates signalling pathways implicated in cellular growth and proliferation such as ERK1/2 and Akt, we examined whether INSL5 influenced cell proliferation rate *in vitro*. Human and mouse INSL5 enhanced BrdU incorporation in CHO-RXFP4 cells in a concentration-dependent

manner (mINSL5: pEC50 = 9.11 ± 0.25; hINSL5: pEC50 = 8.38 ± 0.43; n = 5; Fig. 4), indicating that activation of RXFP4 promotes cell proliferation.

RXFP4 interacts with GRK2, β-arrestin 1, β-arrestin 2 and the early endosome marker Rab5a, and dissociates from membrane bound KRas following INSL5 activation

BRET was used to examine Rluc8-tagged RXFP4 interactions with Venus-tagged G protein receptor kinase 2 (GRK2), β-arrestin 1, β-arrestin 2, Rab5a (early endosome marker) or KRas (plasma membrane marker) following activation by INSL5. Treatment with mouse or human INSL5 (200 nM each) promoted RXFP4 interactions with GRK2 [n = 8 (mINSL5), n = 6 (hINSL5); Fig 5A], β-arrestin 1 [n = 5 (mINSL5), n = 6 (hINSL5); Fig 5B], β-arrestin 2 (n = 5; Fig 5C), and Rab5a (n = 5; Fig 5E) and caused dissociation of the receptor from KRas [n = 8 (mINSL5), n = 5 (hINSL5); Fig 5D], suggesting that RXFP4 undergoes classical GRK phosphorylation and β-arrestin-mediated receptor internalisation, followed by sequestration to early endosomal compartment following ligand stimulation.

INSL5 inhibits glucose-stimulated insulin secretion and calcium mobilisation in MIN6 insulinoma cells and inhibits cAMP accumulation in NCI-H716 enteroendocrine cells.

A previous study showed that INSL5 potentiated glucose-stimulated insulin secretion in MIN6 insulinoma cells and primary murine islets, suggesting that INSL5-RXFP4 may constitute a novel incretin axis similar to GLP1-GLP1R (Luo et al., 2015). We first confirmed that *rxfp4* mRNA is expressed in MIN6 cells using real-time quantitative PCR, though at a markedly lower level than *glp1r* (n = 6; Fig 6A). Next, we investigated the effects of INSL5 on glucose-mediated insulin secretion in MIN6 cells. mINSL5 (0.1 – 200 nM) did not affect the ability of MIN6 to secrete insulin in the absence of glucose stimulation (0 mM glucose; n = 5; Fig 6B). Treatment of MIN6 cells with 10 mM glucose evoked robust insulin secretion that was inhibited by the co-addition of mINSL5 (0.1 and 1 nM; $p < 0.05$; n = 5; Fig 6B). There was evidence of a bell-shaped concentration-response relationship since the inhibitory effect of mINSL5 on glucose-stimulated insulin secretion was lost at higher concentrations of mINSL5. Since Ca^{2+} influx typically occurs in β-cells following a depolarising stimulus (e.g. glucose) and is widely considered an important trigger for the exocytosis of insulin granules, we investigated the effect of mINSL5 on glucose-stimulated Ca^{2+} mobilisation in MIN6 cells. Co-addition of mINSL5 (10^{-9} M) diminished the Ca^{2+} response evoked by 10 mM

glucose whereas co-addition of GLP-1 (10^{-8} M) potentiated the glucose-mediated Ca^{2+} response (Fig 6C). The Ca^{2+} mobilisation experiment was also performed in parallel with different concentrations of mINSL5, and the areas under the curves encompassed by the different treatments quantified ($p < 0.05$ for mINSL5 [10^{-9} M]; $p < 0.01$ for GLP-1; Fig 6D). Our results obtained using two different approaches (insulin secretion and Ca^{2+} mobilisation) suggest that INSL5 does not behave like GLP-1 as it inhibits glucose-stimulated insulin secretion. In addition, we did not observe p-ERK1/2 and cAMP inhibition in response to RXFP4 activation in MIN6 cells as observed in the CHO-RXFP4 system (data not shown). However in NCI-H716 cells - an established human cell model of enteroendocrine cells – hINSL5 (10^{-7} M) inhibited forskolin stimulated cAMP accumulation ($p < 0.01$; $n = 5$; Fig 6E).

Discussion

Mouse INSL5 displayed greater potency than human INSL5 in all of our signalling assays (Table 1), consistent with the higher binding affinity observed for the mouse homologue compared to human INSL5 (Belgi et al, 2013). Under the assay conditions used here, mouse INSL5 was most potent for inhibition of cAMP accumulation, as observed previously using a CRE reporter gene assay (Belgi et al, 2011; Belgi et al, 2013). There is high sequence conservation between the human and mouse peptides, particularly in the long B chain α-helix that extends from Gly^{B8} through to the C-terminal Trp^{B24}. The INSL5 residues that govern activation of RXFP4, Arg^{B13}, Tyr^{B17} and Arg^{B23}, are identical between human and mouse, as are residues making up the hydrophobic core of the folded peptide (Leu^{A3}, Cys^{A7}, Cys^{A12}, Leu^{A17}, Cys^{A21}, Leu^{B6}, Tyr^{B11}, and Val^{B15})(Haugaard-Jonsson et al, 2009). Key differences are found in a series of charged residues that contribute to correct folding of INSL5 via electrostatic interactions and hydrogen bonding. In human INSL5, Asp^{A2} forms hydrogen bonds to amide protons of Gln^{A4} and Thr^{A5} and the side-chain hydroxyl group proton of Thr^{A5}. Asp^{A10} and Asp^{A16} both interact with Lys^{B1}, and there is a weaker interaction between Glu^{B2} and Arg^{B5}. These residues also undergo hydrogen bonding with additional side chain serine and threonine hydroxyl groups or to amide protons (Haugaard-Jonsson et al, 2009). While Asp^{A2} and Gln^{A4} are conserved, Thr^{A5} is an alanine in mouse INSL5, Asp^{A10} is glutamate, Asp^{A16} is also glutamate, and Lys^{B1} is arginine. The last three differences are conservative in nature, but the longer side chain of glutamate compared to aspartate would likely produce subtle differences in the overall structure of INSL5 that contribute to the observed higher affinity of the mouse homologue for human RXFP4. In addition, Glu^{B2} is a glutamine and Arg^{B5} is a lysine in mouse INSL5, so this interaction would be altered. A recent study identifies K^{A15} as a key residue in the A-chain of mouse INSL5 that is responsible for the improved RXFP4 activity compared with human INSL5 (Patil et al., 2016). In a similar fashion, porcine relaxin-2 consistently has higher affinity and potency at the human RXFP1 receptor than human relaxin-2 (Halls, 2004).

Pharmacological blockade of $G\alpha_{i/o}$ by PTX and Src by PP2 completely abolished activation of ERK1/2, Akt and S6RP by mouse INSL5, indicating that $G\alpha_{i/o}$ and Src are upstream of these events and obligatory for RXFP4 signalling. In comparison, the closely related RXFP3 shows partial, but not complete, suppression of H3-relaxin stimulated ERK1/2 activation by PP2 (van der Westhuizen et al., 2007), suggesting that RXFP4 and RXFP3 may activate ERK1/2 in a different manner. Interestingly, RXFP4, but not RXFP3, contains a proline-rich binding motif (PXXP) in

intracellular loop 1 (Vroling et al., 2011) that may permit direct binding of the SH3 domain of Src to the receptor. Indeed, direct interaction with Src has been shown to be critical for β_3-adrenoceptor mediated ERK1/2 activation (Cao, 2000). Whether such an interaction also dictates RXFP4 signalling to ERK1/2 remains to be determined.

Our inhibitor experiments indicate that there is redundancy in some RXFP4 signalling pathways (Figures 2, 7). For example, the MEK1/2 inhibitor U0126 partially inhibits phosphorylation of S6RP despite complete inhibition by KU0063794 and rapamycin, indicating that the primary pathway is via activation of mTORC1. Similarly, LY294002 partially inhibits ERK1/2 phosphorylation. mTOR is not upstream of INSL5-stimulated ERK1/2 activation but is necessary for Akt and S6RP activation. Furthermore, mTORC2, but not mTORC1, is the upstream mediator of Akt activation by RXFP4 since selective inhibition of mTORC1 by rapamycin had no significant effect on the INSL5-stimulated Akt response, which was blocked by combined inhibition of mTORC1 and mTORC2 by KU0063794. This is in accord with previous findings showing that rictor-bound mTOR (mTORC2) is responsible for Akt phosphorylation at Ser473 and facilitates phosphoinositide-dependent kinase-1-mediated Akt phosphorylation at Thr308 (Sarbassov et al., 2005).

The recruitment of $G\alpha_{i/o}$ isoforms to RXFP4 was explored using PTX-insensitive mutants. RXFP4 was able to engage multiple $G\alpha_{i/o}$ isoforms to promote cAMP inhibition and ERK1/2 activation and in this respect resembles RXFP3 (Kocan et al., 2014) with which RXFP4 shares a high degree of homology. The rescue of responses was greater for cAMP than for ERK1/2 responses but there was little distinction between the G protein isoforms suggesting that RXFP4 is quite promiscuous and that the precise pattern of G protein activation may vary with cell type. For RXFP3, studies in CHO cells using PTX-insensitive G protein mutants showed coupling predominantly to $G\alpha_{oB}$ and $G\alpha_{i2}$ whereas in HEK cells $G\alpha_{oA}$ coupling was also observed (van der Westhuizen, 2008). Direct measurement of G protein coupling in CHO cells expressing RXFP3 using BRET showed coupling to $G\alpha_{oA,}$ $G\alpha_{oB,}$ $G\alpha_{i2}$ and $G\alpha_{i3}$ but interestingly activation of the receptor by the biased agonists relaxin and R3(BΔ23-27)R/I5 only caused coupling to $G\alpha_{oB}$ and $G\alpha_{i2}$, perhaps indicating that these are preferred (Kocan et al., 2014). In comparison, the relaxin receptor RXFP1 selectively recruits $G\alpha_{oB}$ and $G\alpha_{i3}$, in addition to $G\alpha_s$, to modulate intracellular cAMP levels (Halls et al., 2006). Unlike RXFP1, the pharmacological actions of RXFP4 are solely $G\alpha_{i/o}$-mediated, since

stimulation with INSL5 alone fails to produce an increase in cAMP level with no $G\alpha_s$ component (data not shown).

Many ligand-activated GPCRs undergo homologous desensitisation involving phosphorylation of serine and threonine residues in the cytoplasmic tail by GRKs, leading to β-arrestin1/2 recruitment and receptor internalisation (DeWire et al., 2007). Here, we show that INSL5 treatment is followed by interaction between RXFP4 and GRK2 and β-arrestin1/2 associated with receptor internalisation and translocation to the early endosome compartment, an effect also observed with ligand-activated RXFP3 (Fig 7) (Kocan et al., 2014). This contrasts with RXFP1 and RXFP2, that lack the ability to recruit β-arrestins and are poorly internalised following receptor stimulation (Callander et al., 2009). Thus RXFP4 behaves somewhat similarly to RXFP3, in BRET interaction studies and in cell signalling assays.

There is evidence to suggest that RXFP4 mRNA is expressed in MIN6 pancreatic β cells and that stimulation by INSL5 activates ERK1/2 (Luo et al., 2015). We confirmed RXFP4 mRNA expression in MIN6, although at a substantially lower level than GLP1R. Our finding that INSL5 inhibits glucose-mediated insulin release and Ca^{2+} response in MIN6, contrasts with the previous study (Luo et al., 2015), which suggested that INSL5 potentiated glucose-stimulated insulin secretion in MIN6 cells and primary islets. However, it is well accepted that increased cAMP and Ca^{2+} levels promote exocytosis of insulin granules in β-cells (for review see Rorsman & Braun, 2013) whereas G_i-coupled receptors such as the growth hormone secretagogue receptor (Dezaki et al., 2007) or the α_2 adrenergic receptor (Gibson et al., 2006) inhibit insulin release. Our finding that RXFP4 is coupled to $G\alpha_{i/o}$ proteins, inhibits cAMP accumulation in the CHO cell system and inhibits Ca^{2+} release and insulin release in MIN6 cells would appear to follow that paradigm. We were also able to show inhibition of cAMP accumulation in entero-endocrine NCI-H716 cells

INSL5 stimulation of RXFP4 activates MAPK pathways and the PI3K-Akt-mTOR-S6RP signalling cascade that are associated with cell proliferation in CHO cells (Fig 7). The roles of ERK1/2 and PI3K-Akt-mTOR signalling in cellular growth, proliferation and metabolism are well documented (Laplante and Sabatini, 2009; Polak and Hall, 2009). S6RP is a downstream effector of mTOR that is involved in protein synthesis, and has been implicated in pancreatic β cell homeostasis as shown by insulin deficiency and smaller β cell size in mice with global knock in of a dominant negative S6RP that lacks all 5 possible phosphorylation sites (Ruvinsky et al., 2005). Interestingly, INSL5 knockout mice also appear to have a reduced number of β cells in the islet of Langerhans

(Burnicka-Turek et al., 2012). Thus it is appealing to suggest that INSL5-RXFP4 may be involved in β cell homeostasis, although more evidence is needed to establish this link.

In this study, CHO-K1 cells stably transfected with RXFP4 were selected as a model to investigate intracellular signalling pathways. Furthermore, CHO-K1 cells have been successfully utilised to characterise signalling pathways activated by a number of recently deorphanised GPCRs, including the closely related RXFP3 (van der Westhuizen et al., 2007; Kocan et al., 2014) and the ghrelin receptor growth hormone secretagogue receptor 1a (Mousseaux et al., 2006). Such expression systems can therefore provide a useful guide to signalling pathways likely to be found in endogenously expressing systems. Currently, cells that endogenously express RXFP4 are not yet well characterised. Nevertheless there is evidence that RXFP4 is mainly expressed in the gastrointestinal tract, particularly in the duodenum, colon and rectum, but interestingly not significantly in the pancreas, as indicated by next generation sequencing of protein coding genes in human tissues (Uhlén et al., 2015). Furthermore, RXFP4 expression in the enteric nervous system has been demonstrated by *in situ* hybridisation, with localisation to submucosal and myenteric nerve plexuses of the colon (Grosse et al., 2014). This would suggest that INSL5, released from L-cells in the gastrointestinal tract, may activate RXFP4 in an autocrine/paracrine manner. Indeed, our cAMP result in the NCI-H716 enteroendocrine cells, and the ERK1/2 result in GLUTag cells (Luo et al., 2015) support this notion.

Altogether, our study demonstrates that INSL5 stimulation of RXFP4 activates a range of signalling cascades which include inhibition of cAMP production, activation of ERK1/2, p38MAPK, Akt and S6RP signalling (Fig 7), which promotes cell proliferation *in vitro*. Activation of RXFP4 also causes interaction with multiple $G\alpha_{i/o}$ proteins and subsequent recruitment of GRK2 and β-arrestins to initiate receptor internalisation. In cells that natively express RXFP4, INSL5 inhibits insulin release and Ca^{2+} mobilisation in MIN6, and inhibits cAMP production in NCI-H716. These findings add to our understanding of RXFP4 signal transduction mechanisms that will be imperative in the development of novel anti-obesity, anti-diabetic and/or appetite-modulating drugs.

Acknowledgements

This work is supported by an Australian National Health and Medical Research Council (NHMRC) program grant (1055134; RJS). DSH is supported by a NHMRC Career Development Fellowship

(545952). SYA is supported by a Faculty of Pharmacy and Pharmaceutical Sciences, Monash University Postgraduate Scholarship. Research at the Florey was supported by an ARC Linkage grant to RADB and MAH (LP120100654) and by the Victorian Government Operational Infrastructure Support Program. RADB is supported by an NHMRC Research Fellowship.

Table 1. pEC_{50} values for human INSL5 and mouse INSL5 activation of ERK1/2 (n = 6), p38MAPK (n = 5), Akt Ser473 (n = 6), Akt Thr308 (n = 6), S6RP (n = 5) and inhibition of cAMP (n = 5 – 7) in CHO-RXFP4 cells. Numbers represent mean of pEC_{50} ± S.E.M. of *n* independent experiments. Lower diagram shows the primary structure of human INSL5 and mouse INSL5. Sequence differences between the peptide orthologues are highlighted by white and black boxes that represent conserved and non-conserved mutations, respectively. Z in the A-chain of human INSL5 corresponds to pyroglutamic acid.

Ligand	ERK1/2	P38MAPK	Akt Ser473	Akt Thr308	S6RP	cAMP
Mouse INSL5	8.54 ± 0.09	8.13 ± 0.20	7.86 ± 0.28	7.80 ± 0.30	8.33 ± 0.24	8.86 ± 0.10
Human INSL5	7.52 ± 0.12	7.62 ± 0.30	< 7	< 7	7.46 ± 0.36	7.68 ± 0.19

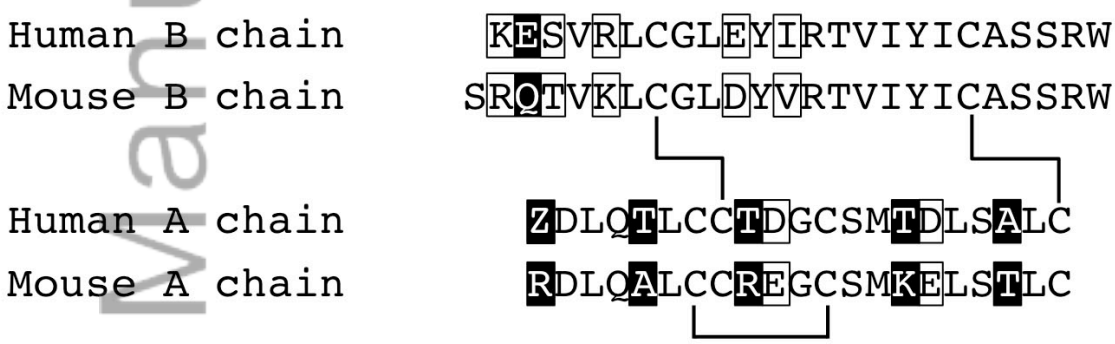

Figure Legends

Figure 1. Concentration-response relationships for activation of ERK1/2, Akt, p38MAPK and S6RP and inhibition of cAMP production by hINSL5 and mINSL5 in CHO-RXFP4 cells. In (A) phosphorylation of ERK1/2 (5 min; n = 6), (B) Akt-Ser473 (5 min; n = 6), (C) Akt-Thr308 (5 min; n = 6), (D) p38MAPK (15 min; n = 5) and (E) S6RP (30 min; n = 5), with in (F) inhibition of forskolin-stimulated cAMP accumulation (30 min; n = 5 (mINSL5), n = 7 (hINSL5)). CHO-RXFP4 cells were treated with increasing concentrations of hINSL5 or mINSL5 (10^{-11} M to $10^{-6.5}$ M). Results are normalised to the maximum response to hINSL5 in protein phosphorylation assays, or % of response to 3 μM forskolin in cAMP accumulation assay. Data points represent mean ± S.E.M. of independent experiments.

Figure 2. Effects of pathway inhibitors on signalling responses to mINSL5 in CHO-RXFP4 cells. CHO-RXFP4 cells were pretreated with the $G\alpha_{i/o}$ inhibitor (PTX; 100ng/ml), MEK inhibitor (U0126; 10 μM), Src family tyrosine kinase inhibitor (PP2; 10 μM), PI3K inhibitor (LY294002; 10 μM) or the mTOR complex inhibitors (KU0063794; 1 μM, rapamycin; 100nM) followed by INSL5 (100 nM). Pathways examined were **(A)** p-ERK1/2, **(B)** Akt p-Ser473 **(C)** Akt p-Thr308 and **(D)** p-S6RP. Cells were treated with inhibitors for 30 min before and then during mINSL5 stimulation, except for the PTX treatment where cells were exposed for 18h. Results are quantified as fold change in fluorescence over that of the vehicle treatment in the control group. Bars represent mean ± S.E.M. of experiments (n = 5 (PTX, LY294002, KU0063794, Rapamycin), n = 6 (PP2, U0126), n = 10 (Control)). Statistical analysis was performed using repeated-measures two-way ANOVA followed by Dunnett's multiple comparisons test. *, $p < 0.05$; **, $p < 0.01$; ***, $p < 0.001$; ****, $p < 0.0001$ versus the mINSL5 response in the control group.

Figure 3. Determination of the $G\alpha_{i/o}$ isoforms utilised by RXFP4 using pertussis toxin resistant Gα mutants. cAMP inhibition and ERK1/2 activation following stimulation by mINSL5 in CHO-RXFP4 cells. RXFP4 inhibits forskolin-stimulated cAMP accumulation indicating an interaction with $G\alpha_{i/o}$ proteins. CHO-RXFP4 cells were transiently transfected with pcDNA3 (mock

transfection) in **(A, G)** or $G_{i/o}$ subunit constructs carrying the C351I mutation in (□, **H)** $mG\alpha_{oA}$, **(C, I)** $mG\alpha_{oB}$, **(D, J)** $mG\alpha_{i1}$, **(E, K)** $mG\alpha_{i2}$ or **(F, L)** $mG\alpha_{i3}$. In the top panels, cells were incubated with PTX (100 ng/ml) for 16 hours and cAMP production stimulated by forskolin (3 μM) followed by treatment with mINSL5 (100 nM). Results are normalised to the cAMP response stimulated by forskolin. In the bottom panels, the ERK1/2 response was measured in cells incubated with PTX (100 ng/ml) for 16 hours followed by treatment with mINSL5 (100 nM). Results are expressed as percentage of response elicited by 10% FBS. Bars represent mean ± S.E.M. of independent experiments (cAMP: n = 6 ($mG\alpha_{oA}$, $mG\alpha_{i3}$), n = 7 (pcDNA3, $mG\alpha_{oB}$, $mG\alpha_{i1}$, $mG\alpha_{i2}$); ERK1/2: n = 5). Statistical analysis was performed using repeated-measures two-way ANOVA followed by Dunnett's multiple comparisons test. *, $p < 0.05$; **, $p < 0.01$; ***, $p < 0.001$; ****, $p < 0.0001$ versus the forskolin response (cAMP inhibition) or the baseline response (ERK1/2 activation) in PTX-treated cells.

Figure 4. Activation of RXFP4 by human INSL5 or mouse INSL5 promotes increased cellular BrdU incorporation. Concentration-response relationships are shown for cellular BrdU incorporation stimulated by hINSL5 or mINSL5 (10^{-12} M to 10^{-8} M) in CHO-RXFP4 cells. Results are expressed as percentage of response elicited by 10% FBS. Data points represent mean ± S.E.M. of independent experiments (n = 5).

Figure 5. Real-time kinetic BRET studies of interactions between RXFP4 and (A) GRK2, (B) β-arrestin 1, (C) β-arrestin 2, (D) membrane bound Kras and (E) early endosome marker Rab5a induced by human and mouse INSL5. CHO-K1 cells were transiently co-transfected with RXFP4-Rluc8 and Venus-tagged GRK2, β-arrestin 1, β-arrestin 2, Rab5a or KRas constructs. Following transfection, cells were stimulated with hINSL5 or mINSL5 (200 nM). Ligand-induced BRET ratios were calculated by subtracting the ratio for the vehicle-treated sample from the BRET ratio for each ligand-treated sample as described. Data points represent mean ± S.E.M. of independent experiments (n = 5 – 8).

Figure 6. INSL5 inhibits glucose-stimulated insulin secretion and calcium mobilisation in MIN6

murine insulinoma cells and cAMP accumulation in NCI-H716 human enteroendocrine cells. In (A) real-time quantitative PCR assay to determine the expression levels of *rxfp4* and *glp1r* that are expressed as ratios relative to *ACTB*, multiplied by 1000 (n = 6). In (B) MIN6 cells were equilibrated for 2 hours in KRB buffer, followed by stimulation in either 0 mM or 10 mM glucose by mINSL5 (0.1 – 200 nM) for 2 hours. Supernatants were assayed for insulin that is expressed in ng/ml (n = 5). In (C) Ca^{2+} mobilisation in MIN6 cells (n = 5) using Fluo-4 AM (1 μM) in response to 10 mM glucose alone or in the presence of mINSL5 (10^{-9} M) or GLP-1 (10^{-8} M). Concentration-response relationships for inhibition of Ca^{2+} responses (AUC) by INSL5 were bell-shaped (D). In (E), NCI-H716 human enteroendocrine cells stimulated with forskolin (3 μM) showed inhibition of cAMP accumulation with hINSL5 (10^{-7} M; n = 5). Data points represent mean ± S.E.M. of n independent experiments. * P<0.05; **P<0.01

Figure 7. RXFP4 signal transduction pathways. Inhibitors used in studying RXFP4 signalling mechanisms are boxed in red. Following INSL5 stimulation, RXFP4 recruits multiple $G\alpha_{i/o}$ subunits (predominantly $G\alpha_{oA}$, $G\alpha_{oB}$, $G\alpha_{i2}$) that activate a range of signalling pathways, including cAMP inhibition, ERK1/2 (Thr202/Tyr204), Akt (Thr308 and Ser473) p38MAPK (Thr180/Tyr182) and S6RP (Ser235/236) via intermediary pathways such as mTORC1/C2, Src, PI3K and MEK1/2 leading to enhanced cell proliferation. Activated RXFP4 interacts with GRK2 and β-arrestins that leads to movement of the receptor away from the plasma membrane into early endosome compartments. Note: speculative pathways are shown with dotted lines. AC, adenylyl cyclase; β-Arr 1/2, β-arrestins 1/2.

References

Alexander S.P.H, Davenport, A.P, Kelly, E, Marrion, N, Peters, J.A, Benson, H.E, *et al.* (2015). The Concise Guide to PHARMACOLOGY 2015/16: G protein-coupled receptors. Br J Pharmacol 172: 5847

Bahia DS, Wise A, Fanelli F, Lee M, Rees S, Milligan G (1998). Hydrophobicity of residue^{351} of the G protein $G_{i1}\alpha$ alpha determines the extent of activation by the α_{2A}-adrenoceptor. Biochemistry 37: 11555–11562.

Belgi A, Bathgate, RA, Kocan M, Patil N, Zhang S, Tregear GW *et al.* (2013). Minimum active structure of insulin-like peptide 5. J. Med. Chem. 56: 9509–9516.

Belgi A, Hossain MA, Shabanpoor F, Chan L, Zhang S, Bathgate RA *et al.* (2011). Structure and function relationship of murine insulin-like peptide 5 (INSL5): free C-terminus is essential for RXFP4 receptor binding and activation. Biochemistry 50: 8352–8361.

Boels K, Schaller HC (2003). Identification and characterisation of GPR100 as a novel human G-protein-coupled bradykinin receptor. Br J Pharmacol 140: 932–938.

Burnicka-Turek O, Mohamed BA, Shirneshan K, Thanasupawat T, Hombach-Klonisch S, Klonisch T *et al.* (2012). INSL5-deficient mice display an alteration in glucose homeostasis and an impaired fertility. Endocrinology 153: 4655–4665.

Callander GE, Thomas WG, Bathgate RA (2009). Prolonged RXFP1 and RXFP2 signaling can be explained by poor internalization and a lack of β-arrestin recruitment. Am J Physiol Cell Physiol 296: C1058–C1066.

Cao W, Luttrell LM, Medvedev AV, Pierce KL, Daniel KW, Dixon TM *et al.* (2000). Direct binding of activated c-src to the β_3-adrenergic receptor is required for MAP kinase activation. J Biol Chem 275: 38131–38134.

Conklin D, Lofton-Day CE, Haldeman BA, Ching A, Whitmore TE, Lok S *et al.* (1999). Identification of INSL5, a new member of the insulin superfamily. Genomics 60: 50–56.

DeWire SM, Ahn S, Lefkowitz RJ, Shenoy SK (2007). β-arrestins and cell signaling. Annu Rev Physiol 69: 483–510.

Dezaki K, Kakei M, Yada T (2007). Ghrelin uses Galphai2 and activates voltage-dependent K+ channels to attenuate glucose-induced Ca2+ signaling and insulin release in islet beta-cells: novel signal transduction of ghrelin. Diabetes 56 (9): 2319-2327.

Fingar DC, Blenis J (2004). Target of rapamycin (TOR): an integrator of nutrient and growth factor signals and coordinator of cell growth and cell cycle progression. Oncogene 23: 3151–3171.

García-Martínez JM, Moran J, Clarke RG, Gray A, Cosulich SC, Chresta CM *et al.* (2009). Ku-0063794 is a specific inhibitor of the mammalian target of rapamycin (mTOR). Biochem J 421: 29–42.

Grosse J, Heffron H, Burling K, Hossain MA, Habib AM, Rogers GJ *et al.* (2014). Insulin-like peptide 5 is an orexigenic gastrointestinal hormone. Proc Natl Acad Sci 111 (30): 33-38

Halls ML, Bathgate RA, Summers RJ (2006). Comparison of signaling pathways activated by the relaxin family peptide receptors, RXFP1 and RXFP2, using reporter genes. J Pharmacol Exp Ther 320: 281–290.

Hossain MA, Bathgate RA, Kong CK, Shabanpoor F, Zhang S, Haugaard Jönsson LM, *et al.* (2008). Synthesis, conformation, and activity of human insulin-like peptide 5 (INSL5). Chembiochem 9: 1816–1822.

Hsu SY (1999). Cloning of two novel mammalian paralogs of relaxin/insulin family proteins and their expression in testis and kidney. Mol Endo 13: 2163–2174.

Jensen DD, Godfrey CB, Niklas C, Canals M *et al.*, (2013). The bile acid receptor TGR5 does not interact with β-arrestins or traffic to endosomes but transmits sustained signals from plasma membrane rafts. J Biol Chem 288:22942-60.

Kocan M, Pfleger KD (2011). Study of GPCR-protein interactions by BRET. Methods Mol Biol 746: 357–371.

Kocan M, Sarwar M, Hossain MA, Wade JD, Summers RJ (2014). Signalling profiles of H3 relaxin, H2 relaxin and R3(BΔ23-27)R/I5 acting at the relaxin family peptide receptor 3 (RXFP3). Br J Pharmacol 171: 2827–2841.

Kocan M, See HB, Seeber RM, Eidne KA, Pfleger KD (2008). Demonstration of improvements to the bioluminescence resonance energy transfer (BRET) technology for the monitoring of G protein–coupled receptors in live cells. J Biomol Screen 13 (9): 888-898.

Laplante M, Sabatini DM (2009). mTOR signaling at a glance. J Cell Sci 122: 3589–3594.

Liu C, Chen J, Sutton S, Roland B, Kuei C, Farmer N, *et al.* (2003). Identification of relaxin-3/INSL7 as a ligand for GPCR142. J Biol Chem 278: 50765–50770.

Liu C, Kuei C, Sutton S, Chen J, Bonaventure P, Wu J, *et al.* (2005). INSL5 is a high affinity specific agonist for GPCR142 (GPR100). J Biol Chem 280: 292–300.

Loewith R, Jacinto E, Wullschleger S, Lorberg A, Crespo, JL, Bonenfant D *et al.* (2002). Two TOR complexes, only one of which is rapamycin sensitive, have distinct roles in cell growth control. Mol Cell 10: 457–468.

Luo X, Li T, Zhu Y, Dai Y, Zhao J, Guo Z *et al.* (2015). The insulinotrophic effect of insulin-like peptide 5 in vitro and in vivo. Biochem J 466: 467–473.

Luttrell LM, Hawes BE, van Biesen T, Luttrell DK, Lansing TJ, Lefkowitz RJ (1996). Role of c-src tyrosine kinase in G protein-coupled receptor- and $G_{\beta\gamma}$ subunit-mediated activation of mitogen-activated protein kinases. J Biol Chem 271: 19443–19450.

Mashima H, Ohno H, Yamada Y, Sakai T, Ohnishi H (2013). INSL5 may be a unique marker of colorectal endocrine cells and neuroendocrine tumors. Biochem Biophys Res Commun 432: 586–592.

Mendoza, MC, Er, EE, Blenis J (2011). The Ras-ERK and PI3K-mTOR pathways: cross-talk and compensation. Trends Biochem Sci 36: 320–328.

Mousseaux D, Le Gallic L, RyanJ, Oiry C, Gagne D, Fehrentz J *et al.* (2006). Regulation of ERK1/2 activity by ghrelin-activated growth hormone secretagogue receptor 1A involves a PLC/PKCε pathway. Br J Pharmacol 148: 350–365.

Offermanns S, Simon MI (1995). Gα15 and Gα16 couple a wide variety of receptors to

phospholipase C. J Biol Chem 270: 15175–15180.

Patil NA, Hughes RA, Rosengren KJ, Kocan M, Ang SY, Tailhades J, *et al.* (2016). Engineering of a Novel Simplified Human Insulin-Like Peptide 5 Agonist. J. Med. Chem 59: 2118-25

Polak P, Hall MN (2009). mTOR and the control of whole body metabolism. Curr Opin Cell Biol *21*: 209–218.

Rorsman P and Braun M (2013). Regulation of Insulin Secretion in Human Pancreatic Islets. Annu Rev Physiol 75: 155-79

Roux PP, Shahbazian D, Vu H, Holz MK, Cohen MS, Taunton J *et al.* (2007). RAS/ERK signaling promotes site-specific ribosomal protein S6 phosphorylation via RSK and stimulates cap-dependent translation. J Biol Chem 282: 14056–14064.

Ruvinsky I, Meyuhas O (2006). Ribosomal protein S6 phosphorylation: from protein synthesis to cell size. Trends Biochem Sci 31: 342–348.

Ruvinsky I, Sharon N, Lerer T, Cohen H, Stolovich-Rain M, Nir T *et al.* (2005). Ribosomal protein S6 phosphorylation is a determinant of cell size and glucose homeostasis. Genes Dev 19: 2199–2211.

Sarbassov DD, Guertin DA, Ali SM, Sabatini DM (2005). Phosphorylation and regulation of Akt/PKB by the rictor-mTOR complex. Science 307: 1098–1101.

Shabanpoor F, Bathgate RA, Wade JD, Hossain MA (2013). C-terminus of the B-chain of relaxin-3 is important for receptor activity. PLoS ONE 8: e82567.

Smith CM, Shen P, Banerjee A, Bonaventure P, Ma S, Bathgate RA, *et al.* (2010). Distribution of relaxin-3 and RXFP3 within arousal, stress, affective, and cognitive circuits of mouse brain. J Comp Neurol 518: 4016–4045.

Sutton SW, Bonaventure P, Kuei C, Nepomuceno D, Wu J, Zhu J *et al.* (2006). G-protein-coupled receptor (GPCR)-142 does not contribute to relaxin-3 binding in the mouse brain: further support that relaxin-3 is the physiological ligand for GPCR135. Neuroendo 82: 139–150.

Gibson TB, Lawrence MC, Gibson CJ, Vanderbilt CA, McGlynn K, Arnette D *et al.* (2006). Inhibition of glucose-stimulated activation of extracellular signal-regulated protein kinases 1 and 2 by epinephrine in pancreatic beta-cells. Diabetes 55 (4): 1066-1073.

Thanasupawat T, Hammje K, Adham I, Ghia J, Del Bigio MR, Krcek J *et al.* (2013). INSL5 is a novel marker for human enteroendocrine cells of the large intestine and neuroendocrine tumours. Oncol Rep 29: 149–154.

Uhlén M, Fagerberg L, Hallström BM, Lindskog C, Oksvold P, Mardinoglu A *et al.* (2015). Tissue-based map of the human proteome. Science 347 (6220): 1260419.

van der Westhuizen ET, Werry TD, Sexton PM, Summers RJ (2007). The relaxin family peptide receptor 3 activates extracellular signal-regulated kinase 1/2 through a protein kinase C-dependent mechanism. Mol Pharmacol 71: 1618–1629.

van der Westhuizen ET (2008). Molecular characterisation of human and mouse relaxin-3 receptors (RXFP3) in recombinant and endogenously expressing cell lines. Ph.D. Thesis, Monash University, Melbourne, Australia.

Vroling B, Sanders M, Baakman C, Borrmann A, Verhoeven S, Klomp J *et al.* (2011). GPCRDB: information system for G protein-coupled receptors. Nucleic Acids Res 39: D309–19.

Tables of Links RXFP4

TARGETS	P38MAP kinase
Other protein targets[a]	S6 ribosomal protein (S6RP)
GRK-2	ERK1
KRAS	ERK2
Rab5a	Akt (PKB)
GPCRs[b]	Src
RXFP4	MEK1/2
Enzymes[d]	mTORC1
Adenylyl cyclase	

LIGANDS
hINSL5
mINSL5
forskolin

These Tables of Links list key protein targets and ligands in this article that are hyperlinked* to corresponding entries in http://www.guidetopharmacology.org, the common portal for data from the IUPHAR/BPS Guide to PHARMACOLOGY (Pawson *et al.*, 2014), and are permanently

archived in *The Concise Guide to PHARMACOLOGY 2015/16* ([a,b,c,d,e]Alexander *et al.*, 2015a,b,c,d,e).

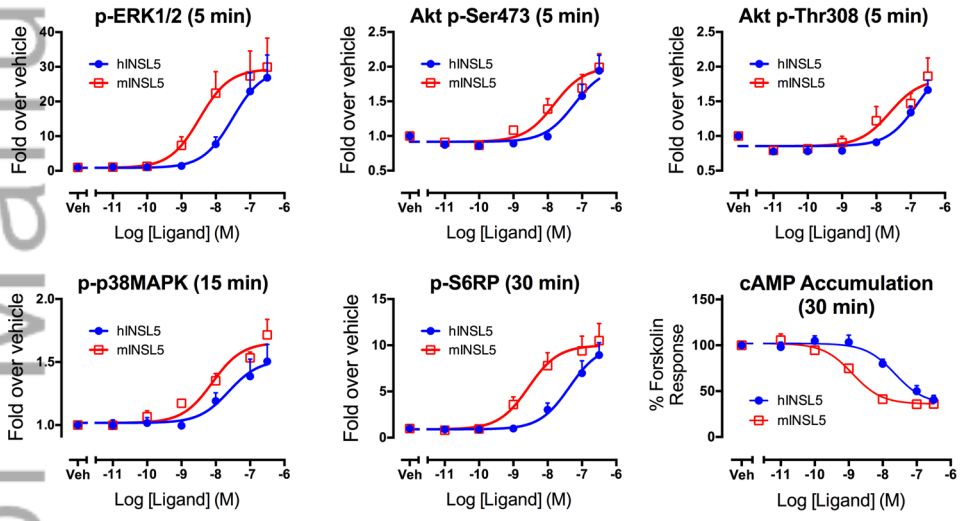

bph_13522_f1

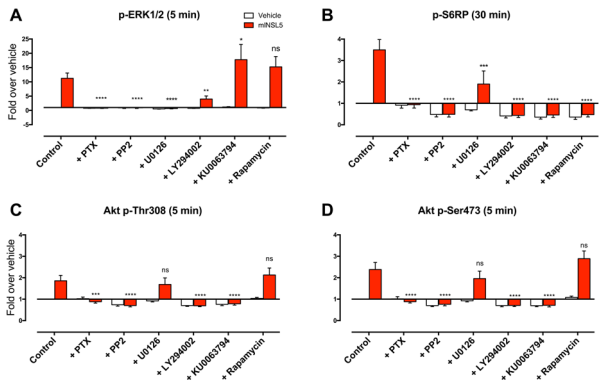

bph_13522_f2

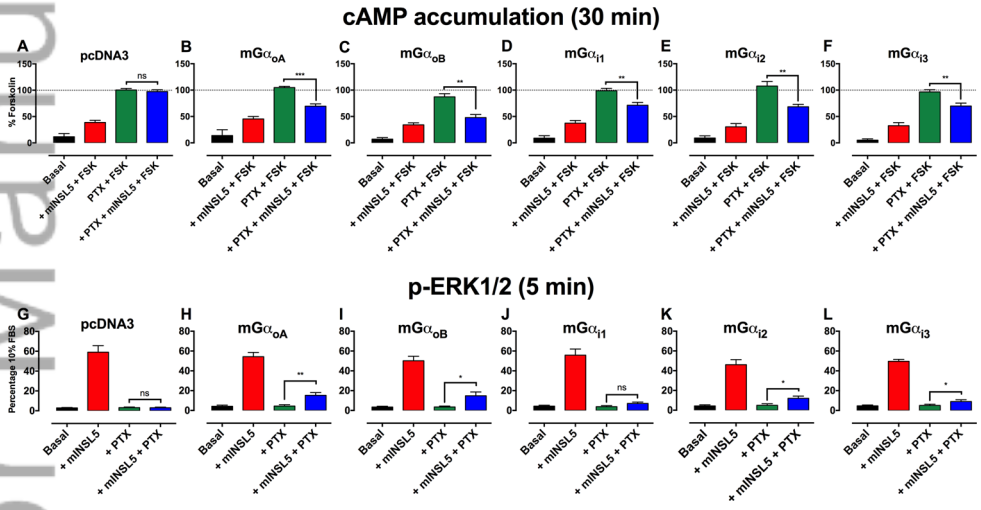

bph_13522_f3

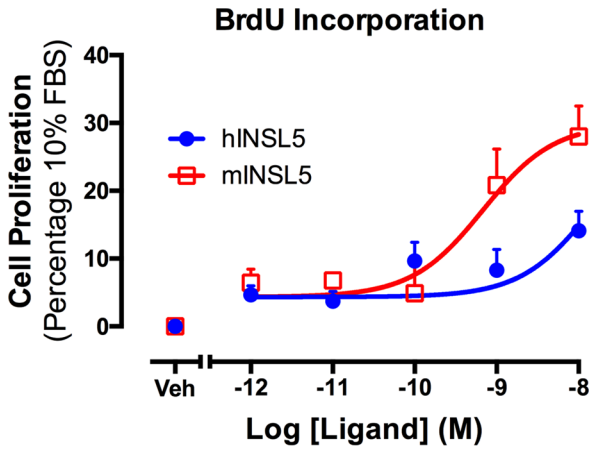

bph_13522_f4

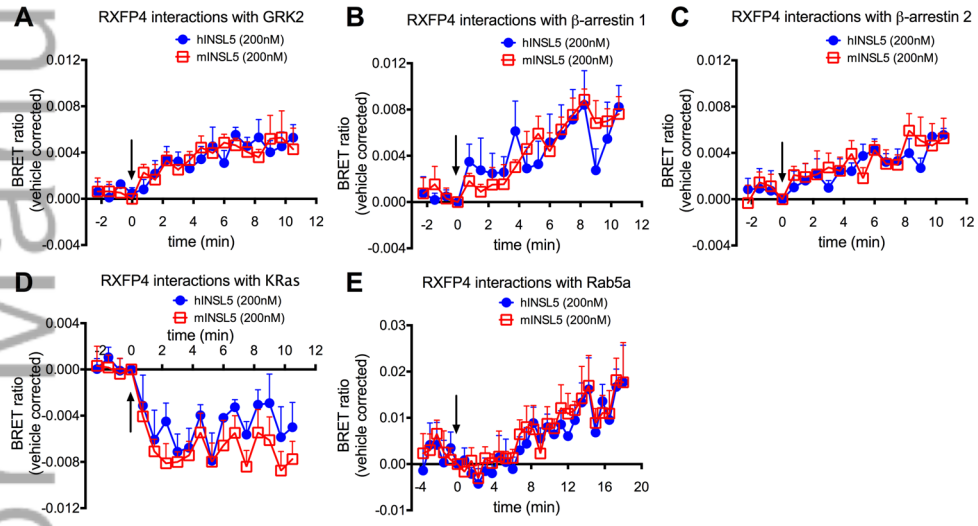

bph_13522_f5

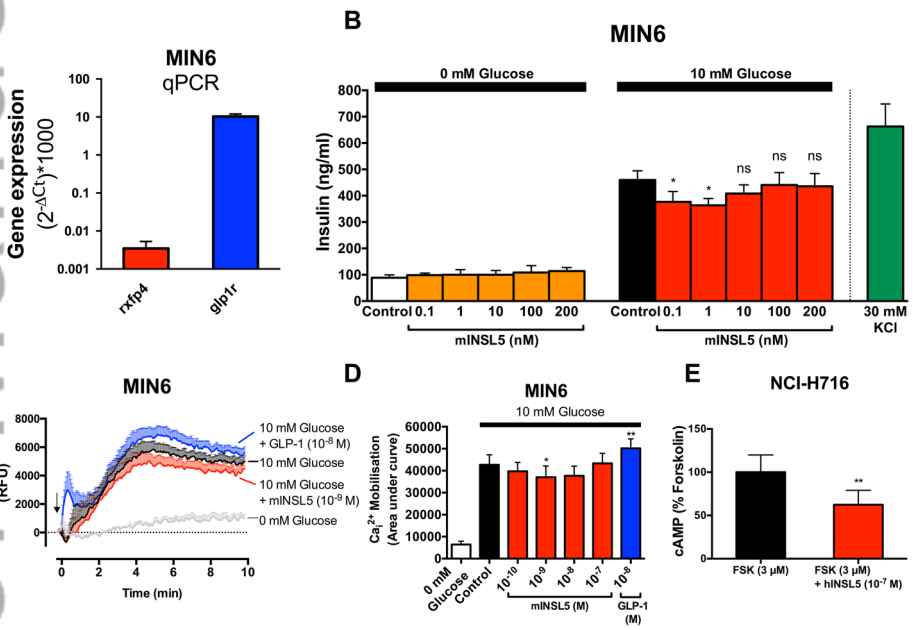

bph_13522_f6

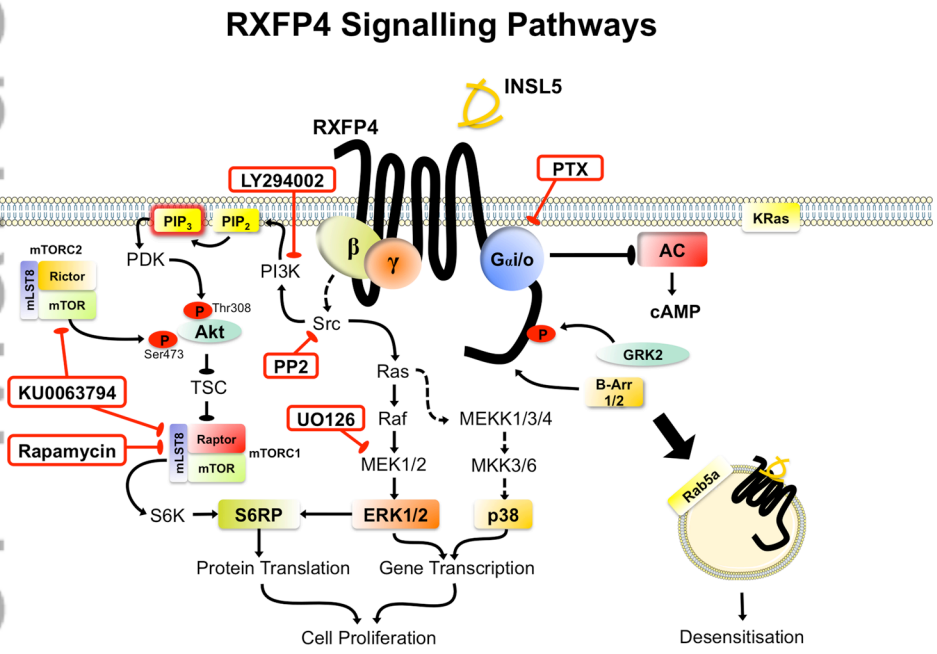

bph_13522_f7